JACS
JOURNAL OF THE AMERICAN CHEMICAL SOCIETY
Article
pubs.acs.org/JACS

Kinetic Stability of the Streptavidin–Biotin Interaction Enhanced in the Gas Phase

Lu Deng,[†] Aron Broom,[‡] Elena N. Kitova,[†] Michele R. Richards,[†] Ruixiang Blake Zheng,[†] Glen K. Shoemaker,[†] Elizabeth M. Meiering,[‡] and John S. Klassen*[,†]

[†]Department of Chemistry and Alberta Glycomics Centre, University of Alberta, Edmonton, Alberta, Canada T6G 2G2
[‡]Department of Chemistry, University of Waterloo, Waterloo, Ontario, Canada N2L 3G1

Supporting Information

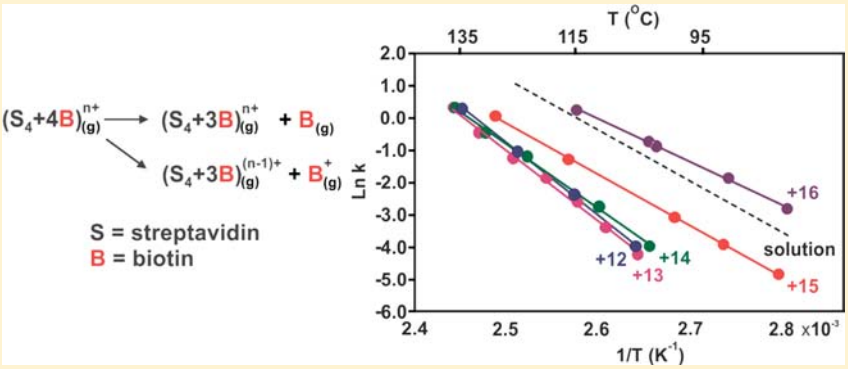

ABSTRACT: Results of the first detailed study of the structure and kinetic stability of the model high-affinity protein–ligand interaction between biotin (B) and the homotetrameric protein complex streptavidin (S_4) in the gas phase are described. Collision cross sections (Ω) measured for protonated gaseous ions of free and ligand-bound truncated (residues 13–139) wild-type (WT) streptavidin, i.e., S_4^{n+} and $(S_4+4B)^{n+}$ at charge states n = 12–16, were found to be independent of charge state and in agreement (within 10%) with values estimated for crystal structures reported for S_4 and (S_4+4B). These results suggest that significant structural changes do not occur upon transfer of the complexes from solution to the gas phase by electrospray ionization. Temperature-dependent rate constants were measured for the loss of B from the protonated $(S_4+4B)^{n+}$ ions. Over the temperature range investigated, the kinetic stability increases with decreasing charge state, from n = 16 to 13, but is indistinguishable for n = 12 and 13. A comparison of the activation energies (E_a) measured for the loss of B from the $(S_4+4B)^{13+}$ ions composed of WT streptavidin and five binding site mutants (Trp79Phe, Trp108Phe, Trp120Phe, Ser27Ala, and Tyr43Ala) suggests that at least some of the specific intermolecular interactions are preserved in the gas phase. The results of molecular dynamics simulations performed on WT $(S_4+4B)^{12+}$ ions with different charge configurations support this conclusion. The most significant finding of this study is that the gaseous WT $(S_4+4B)^{n+}$ ions at n = 12–14, owing to a much larger E_a (by as much as 13 kcal mol^{-1}) for the loss of B, are dramatically more stable kinetically at 25 °C than the (S_4+4B) complex in aqueous neutral solution. The differences in E_a values measured for the gaseous $(S_4+4B)^{n+}$ ions and solvated (S_4+4B) complex can be largely accounted for by a late dissociative transition state and the rehydration of B and the protein binding cavity in solution.

INTRODUCTION

The time scale of noncovalent protein interactions, such as those in protein–receptor, antibody–antigen, and multiprotein complexes, is an important factor in biochemical processes.[1] Relatedly, the lifetime of drug interactions with protein targets strongly influences their pharmacological activity.[2,3] As a result, the ability to predict and control the kinetic stabilities of protein interactions is of fundamental and practical importance. Currently, the relationship between the structures of protein complexes and their association–dissociation kinetics is poorly understood.[1−3] As is the case with structure–affinity relationships, efforts to understand structure–kinetic relationships are generally hampered by solvent effects, which are exceptionally difficult to probe experimentally. Gas-phase studies of desolvated noncovalent protein complexes afford an opportunity to investigate their intrinsic properties, i.e., their structure and kinetic stability, free of solvent effects.[4−13] Furthermore, from a comparison of the structures and stabilities of protein complexes in their hydrated and dehydrated states, it may be possible to gain new insights into the role of water in the binding reactions.[8] Equally important, the results of gas-phase studies of proteins and their complexes serve as important benchmarks to test the reliability of existing computational methods to predict the structure and stability of biological

Received: May 29, 2012
Published: September 17, 2012

interactions and to guide the development of new theoretical tools.

Recently, detailed investigations into the nature and strength of the intermolecular interactions present in the gaseous ions of a limited number of protein−ligand complexes have been reported.[4,6−9,14,15] The best-studied complex is that of a 27 kDa single chain variable fragment (scFv) of the monoclonal antibody Se155-4 and its native trisaccharide ligand (αGal-[αAbe]αMan).[16] The blackbody infrared radiative dissociation−functional group replacement (BIRD-FGR) technique[17,18] was used to identify amino acid residues and sugar hydroxyl groups participating in intermolecular interactions in the gaseous, protonated (scFv+αGal[αAbe]αMan)$^{n+}$ ions over a range of charge states (n = 6−13) and to quantify these interactions.[4,6] Notably, two of the three H-bond donor−acceptor pairs identified at the lower charge states investigated are also present in the available crystal structures. This finding suggests that at least some of the specific intermolecular H-bonds in the (scFv+αGal[αAbe]αMan) complex are conserved upon transfer of the complex from aqueous solution to the gas phase by electrospray ionization (ESI).[6] Moreover, the strengths of the three H-bonds were found to be in good agreement with theoretical values available for model systems.[6] Recently, the BIRD-FGR approach was applied to complexes of bovine β-lactoglobulin (Lg) and a series of long-chain fatty acids (FA).[7−9] Kinetic data for the loss of neutral FAs from deprotonated (Lg+FA)$^{7-}$ ions, together with the results of molecular dynamics (MD) simulations, served as evidence that the acyl chains of the FAs are retained within the hydrophobic ligand binding cavity of Lg in the gas phase.[7] A comparison of the dissociation rate constants measured at 25 °C in the gas phase and in aqueous solution revealed that the (Lg+FA) complexes are more stable kinetically in the absence of solvent.[8] The lower kinetic stability in solution was attributed to the hydration of the FA in the dissociative transition state (TS), which results in a significant reduction in the dissociation activation energy (E_a).[8] Furthermore, a comparison of the gas-phase dissociation E_a values with enthalpies reported for the transfer of hydrocarbons from the gas phase to various organic solvents led to the surprising conclusion that the hydrophobic cavity of Lg is, in fact, relatively polar.[9]

Here, we report on the results of a gas-phase study of the structure and kinetic stability of the streptavidin−biotin (B) interaction, which is among the most stable protein−ligand complexes known and has served as a model system for understanding the origin of high-affinity protein complexes. Streptavidin is a homotetrameric protein complex (S_4) that is isolated from *Streptomyces avidinii*.[19] Each streptavidin subunit consists of 159 residues, which are organized into an eight-stranded β-barrel, one end of which forms the binding site for B.[20] Analysis of crystal structures obtained for the ligand-bound and unbound S_4,[21,22] together with kinetic and thermodynamic data[20,21,23−29] and the results of MD simulations,[30−34] suggests that three structural motifs are responsible for ligand binding: a network of intermolecular H-bonds, van der Waals interactions, and the ordering of surface peptide loops upon binding of B. According to the crystal structures available for the (S_4+4B) complex, B is stabilized by eight H-bonds, involving residues Asn23, Ser27, Tyr43, Ser45, Asn49, Ser88, Thr90, and Asp128 of streptavidin, and the ureido oxygen and nitrogen, the tetrahydrothiophene sulfur, and the carboxyl group of B (Figure 1). Three Trp residues in the binding cavity (Trp79, Trp92, and Trp108), together with Trp120 from the adjacent

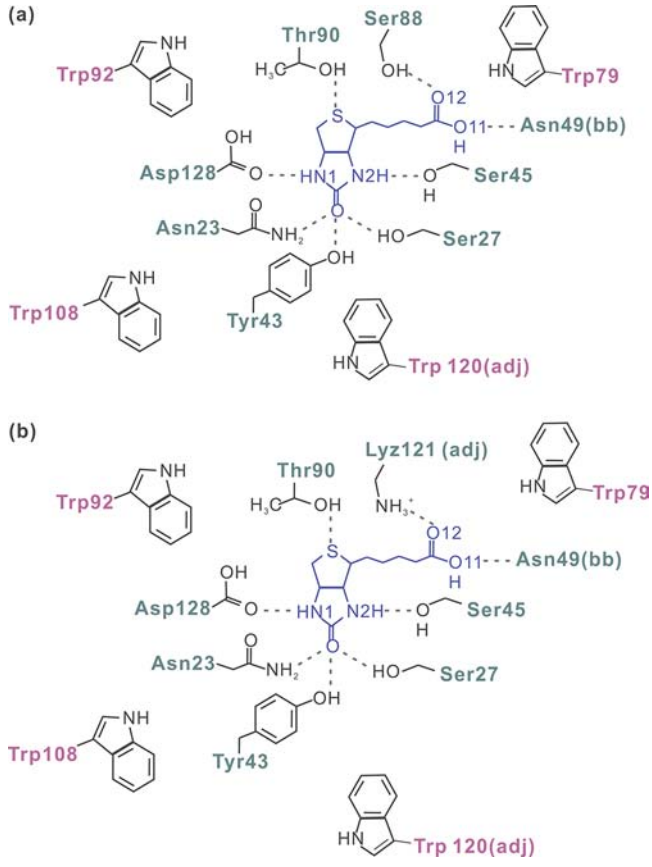

Figure 1. Interaction maps for (a) the WT (S_4+4B) complex obtained from X-ray analysis of the crystal structure and (b) the WT (S_4+B)$^{12+}$ ion determined from MD simulations performed using 15 different charge configurations.

subunit, have been identified as providing an important energetic contribution to the binding of B through van der Waals contacts (Figure 1).[34] In addition, a flexible loop (residues 45−52) on each subunit undergoes a disordered-to-ordered conformational change upon binding of B.[21,28,29]

The unusually slow dissociation of the streptavidin−biotin interaction in aqueous solution is responsible for the exceptionally high affinity ($K_a \approx 10^{14}$ M^{-1} at pH 7.4 and 25 °C).[19,35,36] The origin of the large E_a for ligand escape (31 kcal mol^{-1}),[25] which gives rise to the unusually small dissociation rate constant ($k_{off} = 5.4 \times 10^{-6}$ s^{-1} at pH 7.4 and 25 °C),[27] has been the focus of many experimental[20,21,23−29] and theoretical studies[30−34] but has not been fully explained. Generally, a large E_a is suggestive of a late TS, in which many of the intermolecular interactions are broken or weakened. On the basis of the results of thermodynamic and kinetic studies, it has been proposed that at least four of the intermolecular H-bonds, involving residues Asn23, Ser27, Tyr43, and Asp128, are broken in the TS.[25,26] The H-bond involving Ser45 (in the bound form) is also thought to be cleaved during dissociation but may be replaced with a new H-bond (to the ureido oxygen) in the TS.[24,26] It has also been proposed that the interactions involving Trp79 and Trp120, but not Trp108, are absent in the TS.[27]

Solvent is also expected to influence the magnitude of E_a (and k_{off}), although the nature of the solvent effects is unclear. Stayton and co-workers have suggested that the dissociative TS is free of substantial hydration effects.[27] However, if the loss of

dx.doi.org/10.1021/ja305213z | J. Am. Chem. Soc. 2012, 134, 16586−16596

B from (S_4+4B) complex proceeds by a late TS, rehydration of B and newly exposed residues in the binding cavity will serve to partially offset the energetic penalty of cleaving the protein−ligand interactions and, thereby, lower the E_a. Analysis of the crystal structures of the free and ligand-bound S_4 offers few clues as to the extent of solvent reorganization upon ligand binding.[21,22] A limited number of water molecules (2−4) can be identified in the binding cavity of some subunits of unbound wild-type (WT) S_4, but no water molecules are evident in the bound form.[21,22] However, the limited number or complete absence of crystallographic waters does not necessarily provide an accurate assessment of the extent of hydration of the binding cavity and changes in hydration resulting from ligand binding. Indeed, on the basis of the results of a joint computational and crystallographic study of the earliest dissociation events, it was suggested that loss of B is initiated by the intercalation of a water molecule, which enters the binding site through an access channel at the bottom of the cavity, into the H-bond between B and Asp128.[37] The results of MD simulations reported by Houk and co-workers indicate that, for free streptavidin in an open conformation, seven water molecules reside within the binding cavity.[31] Similar results were reported by Kovalenko and co-workers.[33] Moreover, a single immobilized water molecule, acting as a water bridge between the sulfur and one of the NH groups of B, was identified in the binding cavity of the streptavidin−biotin complex.[33] Together, these computational results suggest that the loss of B is accompanied by the rehydration of the binding cavity by six water molecules.

With the goal of more fully elucidating the influence of solvent on the streptavidin−biotin interaction and the mechanism and kinetics of ligand escape, we have, in the present study, interrogated the structure and kinetic stability of protonated ions of the (S_4+4B) complex, composed of a truncated form of WT streptavidin, in the gas phase. Collision cross sections (Ω) of protonated gaseous ions of the free and ligand-bound streptavidin, i.e., WT S_4^{n+} and WT $(S_4+4B)^{n+}$ at n = 12−16, were determined from ion mobility (IM) measurements and the values compared to the Ω values calculated for the crystal structure reported for WT S_4 and the WT (S_4+4B) complex to establish whether structural changes accompany the transfer of the complexes to the gas phase by ESI. Thermal rate constants for the loss of B from the gaseous WT $(S_4+4B)^{n+}$ ions, at n = 12−16, were measured using the BIRD technique and the Arrhenius parameters established for the loss of neutral and protonated B. The E_a value for the loss of neutral B from WT $(S_4+4B)^{13+}$ ion was compared with those measured for $(S_4+4B)^{13+}$ ions composed of five binding site mutants (Trp79Phe, Trp108Phe, Trp120Phe, Ser27Ala, and Tyr43Ala) to establish whether specific intermolecular interactions are preserved in the gas phase. To aid in the interpretation of the gas-phase data, MD simulations were carried out on desolvated WT $(S_4+4B)^{12+}$ ions with different charge configurations and the streptavidin−biotin interactions identified. Finally, the E_a values for the loss of B from the protonated WT $(S_4+4B)^{n+}$ ions were compared with those measured for the loss of B from the (S_4+4B) complex in aqueous solution in order to assess the possible influence of solvent reorganization on the dissociation kinetics.

EXPERIMENTAL SECTION

Proteins and Biotin. The plasmid for natural core streptavidin (containing residues 13−139 of WT streptavidin, MW 13 271 Da) was a gift from Prof. P. Stayton (University of Washington). Notably, the kinetic data for the dissociation of the (S_4+4B) complex in aqueous solution were measured using natural core streptavidin.[25,27] A QuikChange II site-directed mutagenesis kit (Stratagene, La Jolla, CA) was used to generate the single-site mutants (Trp79Phe, Trp108Phe, Trp120Phe, Ser27Ala, and Tyr43Ala). The PCR step was performed in an MJ Mini PTC-1148 thermocycler (Bio-Rad). The plasmid pET23a vector harboring the streptavidin gene was used as a template. The PCR reaction mixture was treated with 1 μL of *Dpn*I (10 units μL^{-1}) for 60 min at 37 °C to digest template-methylated nonmutated plasmid DNA. The *Dpn*I-treated plasmids were transformed into *E. coli* XL10-Gold cells. Selected transformants were screened for the presence of the recombinant plasmid by restriction mapping and DNA sequence analysis. Positive mutants were transformed into *E. coli* BL21 (DE3) cells for expression. The WT and mutant streptavidin proteins were expressed in *E. coli* and purified using procedures described elsewhere.[38] Solutions of purified S_4 were exchanged directly into 100 mM aqueous ammonium acetate buffer using an Amicon microconcentrator with a MW cutoff of 10 kDa and lyophilized. Stock solutions of S_4 (100 μM) were prepared by dissolving a known amount of lyophilized streptavidin into 100 mM ammonium acetate and stored at −20 °C until needed.

Bovine β-lactoglobulin (Lg, MW 18 363 Da), human plasma transthyretin (TTR, MW 13 922 Da), egg white avidin (Avidin, MW 15 636 Da), *Canavalia ensiformis* concanavalin A (ConA, MW 25 741 Da), and biotin (B, MW 244.3 Da) were purchased from Sigma-Aldrich Canada (Oakville, Canada). Stock solutions of Lg, TTR, Avidin, and ConA (100 μM) were prepared by exchanging each protein into 100 mM ammonium acetate using Vivaspin 500 centrifugal concentrators (Sartorius Steddin Biotech) with a MW cutoff of 10 kDa. The stock solution of B (800 μM) was prepared by dissolving B in Milli-Q water. All stock solutions were stored at −20 °C until needed.

For the IM measurements, the ESI solutions of the calibrant proteins (Lg, TTR, Avidin, and ConA) were prepared at a protein concentration of 10 μM in a 10 mM ammonium acetate buffer. The ESI solution of WT S_4 was prepared at a concentration of 10 μM, with 4 mM imdazole and 10 mM ammonium acetate, while the ESI solution of WT (S_4+4B) also contained 44 μM B. For the gas-phase kinetic measurements, the ESI solutions containing S_4 (10−15 μM) and B (44−66 μM) in 10 mM ammonium acetate (pH 6.8) were prepared from aqueous stock solutions. Where a reduction of charge state for the gaseous $(S_4+4B)^{n+}$ was desired, imidazole (2−8 mM) was added to the solution.[39] To shift the $(S_4+4B)^{n+}$ ions to higher charge states, ESI was performed using a custom-built device that directs a high-velocity flow of air at end of the ESI tip.[40] The choice of using protonated ions, instead of the deprotonated ions, for the present study reflects the ease with which adduct-free $(S_4+4B)^{n+}$ ions can be produced by ESI. In negative ion mode, the deprotonated $(S_4+4B)^{n-}$ ions are produced with extensive acetate adducts, which complicates the interpretation of the kinetic data.

Mass Spectrometry. The gas-phase kinetic measurements were performed using an ApexII 9.4T Fourier transform ion cyclotron resonance mass spectrometer (Bruker, Billerica, MA). Nanoflow ESI was performed on both instruments using borosilicate tubes (1.0 mm o.d., 0.68 mm i.d.), pulled to ∼5 μm o.d. at one end using a P-97 micropipet puller (Sutter Instruments, Novato, CA). The electric field required to spray the solution in positive ion mode was established by applying a voltage of 1.0−1.6 kV to a platinum wire inserted inside the glass tip. The solution flow rate was typically ∼20 nL min^{-1}. Details of the instrumental and experimental conditions used for the BIRD measurements can be found elsewhere.[6,7] The IM measurements were performed using a Synapt G2 quadrupole/ion mobility separation time-of-flight (ESI-Q-IM-TOF) mass spectrometer (Waters, UK). A cone voltage of 40 V was used, and the source block temperature was maintained at 70 °C. Other important voltages for ion transmission, that is, the injection voltages into the trap, ion-mobility, and transfer ion guides, were maintained at 10, 26, and 5 V, respectively. Argon was used in the trap and transfer ion guides at pressures of 2.44×10^{-2} and 3.36×10^{-2} mbar, respectively. The helium chamber preceding the traveling wave IM separation device was maintained at a pressure of

Scheme 1. Dissociation Pathways Observed for the Gas-Phase Ions (a) $(S_4+4B)^{12+}$, (b) $(S_4+4B)^{13+}$, (c) $(S_4+4B)^{14+}$, (d) $(S_4+4B)^{15+}$, and (e) $(S_4+4B)^{16+}$

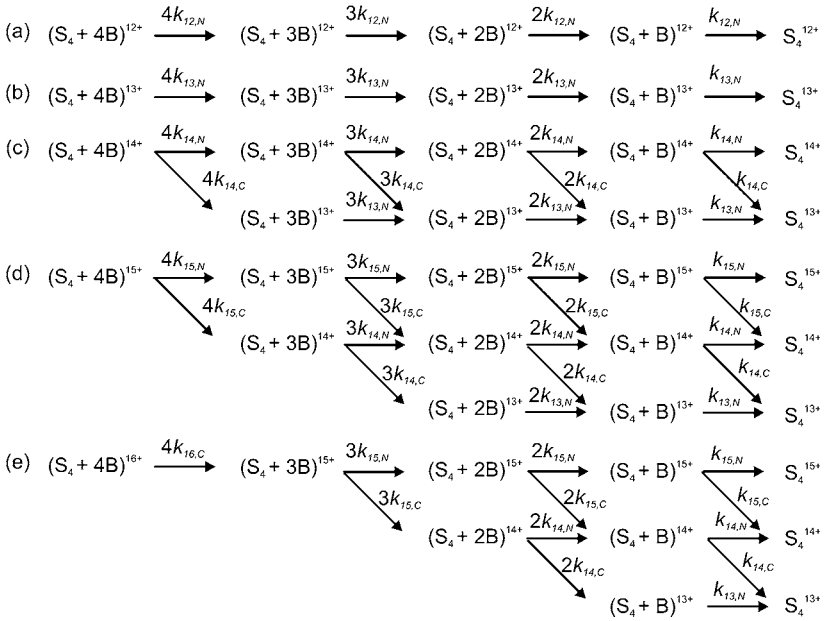

8.90 mbar. All IM measurements were carried out using N_2 as the mobility gas at a pressure of 2.35 mbar. A linear IM T-wave with a fixed wave height of 11 V and velocity of 300 m s^{-1} was used. Data acquisition and processing were carried out using Masslynx (v4.1). Mass spectra were calibrated using a sodium cesium iodide calibration file.

■ COMPUTATIONS

MD simulations were performed using the Amber 11 program suite[41] (Accelrys, San Diego, CA). As there is no available crystal structure of the WT streptavidin−biotin tetramer, the initial geometry of the WT (S_4+4B) complex was obtained by applying a crystallographic symmetry operator on the crystal structure of WT streptavidin−biotin dimer (PDB ID: 3RY2).[22] Each of the tetrameric chains (containing residues 14−134 for the A and C chains, residues 15−136 for the B and D chains) was extended to have the same length as the truncated form (containing residues 13−139) of the WT streptavidin used experimentally. This was done by aligning each tetrameric chain against the C-chain of the crystal structure for streptavidin mutant Ser27Ala (PDB ID: 1N9M)[42] using the DALI server[43] and grafting the extended residues onto each chain of the tetramer. Currently with Amber, atomic charges and atom type parameters are available only for the charged forms of the Arg, C-terminal Ser, and N-terminal Ala residues. Consequently, it was necessary to develop charges and parameters for the neutral forms of Arg, C-terminal Ser, and N-terminal Ala. The charge parameters of the neutral forms of Arg, C-terminal Ser, and N-terminal Ala were parametrized as tripeptides (NME-Arg-ACE, NME-Gly-CSer, and NAla-Gly-ACE, respectively) using the RESP ESP charge derive server (RED Server),[44,45] using Gaussian C.01[46] and enforcing net neutrality across the residue. Ions of the WT (S_4+4B) complex at the +12 charge state were chosen for investigation. As described in more detail below, 15 different charge distributions were considered. Topology and coordinate files for the simulations of each charge distributions were created using the Antechamber module of the AmberTools (version 11).[47] The MD simulations were performed using the Amber 03 force field[48] for streptavidin and a general Amber force field (GAFF)[49] for B. Simulations were performed using a 2 fs time step with bonds to hydrogens constrained using SHAKE. The NVT ensemble was used with an Anderson thermostat (300 K, collision frequency 1 ps^{-1}) and no nonbonded cutoff (full nonbonded interactions). The system was minimized using 500 steps of steepest descent and 500 steps of conjugate gradient minimization. Following minimization, 10 ns of dynamics was needed to fully equilibrate the system, as judged by C_α root-mean-square deviation (rmsd). Following this 10 ns of equilibration, a further 10 ns of production was performed and used in the analysis.

Data Analysis. *Collision Cross Sections.* Determination of Ω from drift time measurements was carried out using protocols described elsewhere.[51,52] Briefly, proteins (Lg, TTR, Avidin, and ConA) with known Ω (in He) were analyzed under the same experimental conditions to establish a correlation between the measured drift times (t_D) and Ω. The t_D values were corrected for both mass-dependent and mass-independent flight times using eq 1:[51]

$$t_D' = t_D - c\sqrt{m/z}/1000 - 10l_{transfer}/WV_{transfer} \quad (1)$$

where t_D' is the corrected drift time (in ms), t_D is the measured drift time (in ms), the constant c is known as the enhanced duty cycle delay coefficient and is found within the Synapt G2 software,[51] $l_{transfer}$ is the length of the transfer T-wave region (in cm), and $WV_{transfer}$ is the transfer wave velocity (in m s^{-1}). The reported Ω (in He) values for the calibrant protein ions[50] were corrected for charge and reduced mass (μ) by eq 2:

$$\Omega' = \Omega\sqrt{\mu}/z \quad (2)$$

where Ω′ is the corrected collision cross section in He. The $t_D'$and Ω′ values of each calibrant ion are summarized in Table S1 (Supporting Information). As shown in Figure S1a, the plot of $\ln(\Omega')$ versus $\ln(t_D')$ is linear. The slope of the curve (0.5712) corresponds to the exponential factor, X, which is sensitive to many experimental variables, including the height and velocity of the voltage "waves" used to propel ions through

dx.doi.org/10.1021/ja305213z | J. Am. Chem. Soc. 2012, 134, 16586−16596

the IM separation region.[53] Using the empirically determined value of X, the final, corrected drift times (t_D'') were established using eq 3:

$$t_D'' = (t_D')^X (z/\sqrt{\mu}) \quad (3)$$

Notably, the plot of literature Ω values versus t_D'' is linear, with an R^2 value of 0.997 (Figure S1b). The Ω values of the protonated WT S_4^{n+} and WT $(S_4+4B)^{n+}$ ions were determined from the calibration curve and the corresponding t_D'' values.

The Ω values for WT S_4 and (S_4+4B) in aqueous solution were estimated from available crystal structures using a modified version of Mobcal,[54] which increases the number of iterative calculations performed per input structure and is capable of accepting input coordinate files that contain up to 100 000 atoms, and the trajectory method (TM). The input file for S_4 was prepared using the crystal structure of WT streptavidin tetramer (PDB ID: 1SWB);[21] the input file for (S_4+4B) was prepared as described in the Experimental Section using the crystal structure of WT streptavidin−biotin dimer (PDB ID: 3RY2).[22] The coordinates for the full tetramer were obtained by applying a crystallographic symmetry operator. All crystallographic water molecules were removed manually, and hydrogens were added to the crystal structure using Leap in Amber.[41]

Dissociation Kinetics. The apparent rate constant ($k_{n,app}$) for the loss of B from a given protonated $(S_4+4B)^{n+}$ ion, at a given temperature, was determined from a linear least-squares fit of the plot of the natural logarithm of the normalized abundance (A_R) of the reactant ion versus reaction time. The value of A_R was calculated using eq 4:

$$A_R = \mathrm{Ab}_{(S_4+4B)^{n+}} / \sum \mathrm{Ab}_{(S_4+iB)} \quad (4)$$

where $\mathrm{Ab}_{(S_4+4B)^{n+}}$ is the measured abundance of the $(S_4+4B)^{n+}$ reactant ion and $\sum \mathrm{Ab}_{(S_4+iB)}$ is the total abundance of the reactant and product ions, i.e., all $(S_4+iB)^{n+}$ ions with $0 \le i \le 4$ and, if any, all $(S_4+iB)^{(n-1)+}$ ions with $0 \le i \le 3$. As outlined in Scheme 1, dissociation of the higher charge state $(S_4+iB)^{n+}$ ions proceeds by the loss of both neutral and protonated B through parallel pathways, eqs 5a and 5b:

$$(S_4 + iB)^{n+} \rightarrow (S_4 + (i-1)B)^{n+} + B \quad (5a)$$

$$\rightarrow (S_4 + (i-1)B)^{(n-1)+} + B^+ \quad (5b)$$

For a given protonated $(S_4+4B)^{n+}$ ion, $k_{n,app}$ reflects the intrinsic rate constants for the individual neutral and charged B-loss pathways, $k_{n,N}$ and $k_{n,C}$, respectively, and the number of bound ligands, eq 6:

$$k_{n,app} = 4(k_{n,N} + k_{n,C}) \quad (6)$$

In principle, $k_{n,N}$ and $k_{n,C}$ can be determined from the relative abundance of the unbound S_4^{n+} ion measured once the reaction has gone to completion ($\mathrm{Ab}_{S_4}^{n+\infty}$) and $k_{n,app}$, eq 7:

$$\mathrm{Ab}_{S_4}^{n+\infty} = \left(\frac{k_{n,N}}{k_{n,N} + k_{n,C}}\right)^4 = \left(\frac{4k_{n,N}}{k_{n,app}}\right)^4 \quad (7)$$

However, due to ion losses associated with long trapping times, it is difficult to reliably measure $\mathrm{Ab}_{S_4}^{n+\infty}$, particularly at low reaction temperatures. Therefore, an alternative approach, based on the measured abundances of the reactant and product ions, was used. Using the measured abundances and the corresponding branching ratio, $k_{n,N}/(k_{n,N} + k_{n,C})$, the normalized abundance of S_4^{n+} expected at the completion of the reaction ($\mathrm{Ab}_{S_4}^{n+\infty}$) can be calculated at any point during the reaction, eq 8:

$$\mathrm{Ab}_{S_4}^{n+\infty} = \sum_{i=0}^{4} \left(\frac{k_{n,N}}{k_{n,N} + k_{n,C}}\right)^i \mathrm{Ab}_{(S_4+iB)^{n+}} = \sum_{i=0}^{4} \left(\frac{4k_{n,N}}{k_{n,app}}\right)^i \mathrm{Ab}_{(S_4+iB)^{n+}} \quad (8)$$

where $\mathrm{Ab}_{(S_4+iB)^{n+}}$ is the normalized abundance of the $(S_4+iB)^{n+}$ ion.

Combining eqs 7 and 8 gives eq 9:

$$\left(\frac{4k_{n,N}}{k_{n,app}}\right)^4 = \sum_{i=0}^{4} \left(\frac{4k_{n,N}}{k_{n,app}}\right)^i \mathrm{Ab}_{(S_4+iB)^{n+}} \quad (9)$$

Using the values of $\mathrm{Ab}_{(S_4+iB)^{n+}}$ and $k_{n,app}$ measured at different reaction times, the corresponding values of $k_{n,N}$ were determined by solving eq 9 using Maple (Maplesoft, Waterloo, Canada). At each temperature, $k_{n,N,ave}$ and $k_{n,C,ave}$, the average values of $k_{n,N}$ and $k_{n,C}$, were determined. For the lower charge state $(S_4+4B)^{n+}$ ions, with n = 12 and 13, where B is lost only at its neutral form, $k_{n,N}$ is simply equal to $^1/_4\, k_{n,app}$, while for the $(S_4+4B)^{16+}$ ion, which dissociates exclusively (or nearly so) by the loss of protonated B, $k_{n,C}$ is equal to $^1/_4\, k_{n,app}$.

Computational Results. Trajectory analysis, performed using the Visual Molecular Dynamics package,[55,56] was carried out to establish the C_α rmsd for streptavidin, the angles and distances associated with the H-bonds between B and streptavidin, and the distances associated with the intermolecular van der Waals interactions between B and four tryptophan residues, Trp 79, Trp92, Trp108, and (adjacent subunit) Trp120. In order to determine the number of H-bonds, all potential H-bonding partners between B and streptavidin were scanned at each frame, with the criteria for a H-bond being a heavy-atom distance ≤4 Å and a donor−hydrogen−acceptor angle ≥120°. The total number of H-bonds for each configuration was then averaged across all frames and the four subunits. Additionally, the occupancy, i.e., the fraction f of the simulation steps for which the H-bond criteria are satisfied, was evaluated. All potential van der Waals interaction atom pairs between B and four tryptophan residues (Trp 79, Trp92, Trp108, and Trp120 from adjacent subunit) were scanned at each frame, with the criterion for the presence of van der Waals interactions being that the distance between atom centers for each pair of atoms between relevant tryptophan residue and B is less than or equal to the sum of the van der Waals radii for those particular atoms (van der Waals radii based on the Amber parameter set were used for the simulations). The fraction f of the simulation steps for which the van der Waals interaction criteria are satisfied was also evaluated.

The Ω for the averaged coordinates of the $(S_4+4B)^{12+}$ ion, at each charge configuration, was calculated using Mobcal[54] and the trajectory method (TM). The averaged coordinates were generated by aligning the backbone atoms across all frames, following which the atomic positions were averaged. As side-chain positions can often become distorted due to structural averaging, energy minimization with the protein backbone

dx.doi.org/10.1021/ja305213z | J. Am. Chem. Soc. 2012, 134, 16586−16596

atoms fixed was performed using NAMD[56,57] in order to remove any structural artifacts introduced during the averaging step.

RESULTS AND DISCUSSION

Structure and Kinetic Stability of $(S_4+4B)^{n+}$ Ions in the Gas Phase. Protonated gas-phase ions of WT (S_4+4B) complex, e.g., $(S_4+4B)^{n+}$ at n = 12−16, were produced from aqueous ammonium acetate solutions (10 mM, pH 6.8) containing WT S_4 (10 μM), B (44 μM) and imidazole (4 mM). A representative ESI mass spectrum is shown in Figure 2;

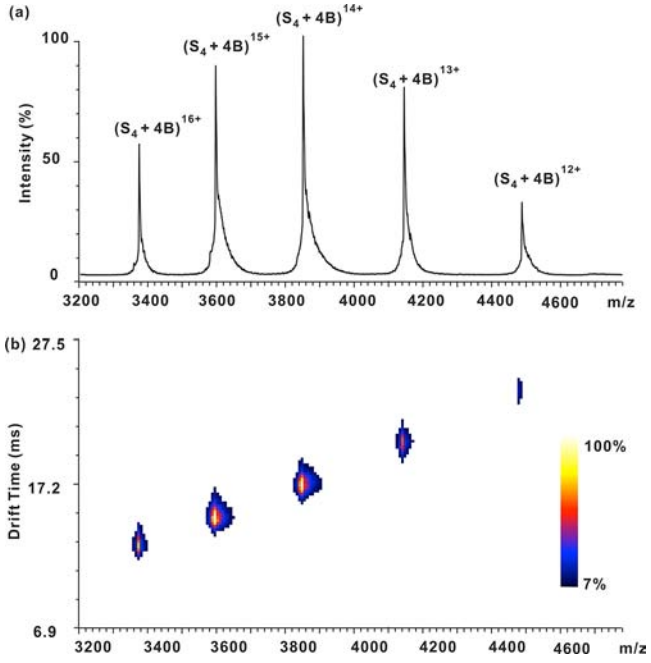

Figure 2. (a) ESI mass spectrum acquired for a neutral aqueous ammonium acetate (10 mM) solution of WT S_4 (10 μM), B (44 μM), and imidazole (4 mM). (b) Ion mobility heat map plotting arrival time versus m/z. The normalized ion intensities (from 7% to 100%) are represented using the indicated color scale.

also shown are the corresponding arrival time distributions measured for the WT $(S_4+4B)^{n+}$ ions. Mobility measurements were also performed on the protonated WT S_4^{n+} ions at n = 12−16, which were produced from aqueous ammonium acetate solutions (10 mM, pH 6.8) containing WT S_4 (10 μM) and imidazole (4 mM), Figure S2. The Ω values for the S_4^{n+} and $(S_4+4B)^{n+}$ ions were determined from their measured drift times and the calibration curve, as described in the Data Analysis section, and are listed in Table 1, together with the Ω values estimated for the crystal structures of WT S_4 and WT (S_4+4B).[21,22]

Interestingly, the Ω values measured for the S_4^{n+} and $(S_4+4B)^{n+}$ ions are independent of charge state, with average values of 34.4 ± 0.1 and 35.0 ± 0.1 nm^2, respectively. These results suggest that charge-induced structural changes, at least over this range of charge states, are minimal. The average Ω value for WT $(S_4+4B)^{n+}$ is 35.0 ± 0.1 nm^2, which agrees within 10% with the Ω value (38.4 ± 0.4 nm^2) estimated for the (S_4+4B) crystal structure. Similar agreement is found between the average Ω value for WT S_4^{n+} (34.4 ± 0.1 nm^2) and the estimated Ω value (38.8 ± 0.4 nm^2). Given that the uncertainty in the Ω values derived from the IM measurements is 5−8%[51]

Table 1. Comparison of Experimentally Estimated Collision Cross Sections (Ω) for the Gaseous S_4^{n+} and $(S_4+4B)^{n+}$ Ions, Where n = 12−16, with Ω Values Calculated for Crystal Structures Reported for S_4 and the (S_4+4B) Complex

	Ω (nm^2)	
charge state n	S_4^{n+}	$(S_4+4B)^{n+}$
12	34.54 ± 0.03[a]	35.08 ± 0.15[a]
13	34.42 ± 0.10[a]	34.99 ± 0.02[a]
14	34.29 ± 0.04[a]	34.88 ± 0.03[a]
15	34.27 ± 0.13[a]	34.78 ± 0.04[a]
16	34.45 ± 0.09[a]	35.03 ± 0.13[a]
average	34.39 ± 0.13[b]	34.95 ± 0.14[b]
crystal structure	38.76 ± 0.37[c]	38.45 ± 0.36[d]

[a]Uncertainty corresponds to the standard deviation of three replicate measurements. [b]Uncertainty corresponds to the standard deviation of the Ω values determined at charge states +12 to +16. [c]Ω was determined from crystal structure (PDB ID: 1SWB) using Mobcal and the trajectory method (TM). [d]Ω was determined from crystal structure (PDB ID: 3RY2) using the TM; the reported error corresponds to one standard deviation of values from replicate (10) calculations.

and the uncertainty in the calculated Ω values is 3−4%, the differences between the Ω values for the $(S_4+4B)^{n+}$ and S_4^{n+} ions and those for the corresponding crystal structures are not significant. Therefore, the IM results would seem to suggest that the transfer of S_4 and (S_4+4B) from neutral aqueous solution to the gas phase by ESI is not accompanied by large structural changes, or at least none that can be identified from the IM measurements.

Time-resolved BIRD measurements were performed on the WT $(S_4+4B)^{n+}$ ions, with n = 12−16, at temperatures ranging from 80 to 135 °C. At these temperatures, BIRD results in the sequential ejection of B, with no evidence for the loss of subunits (Figure S3). The absence of measurable subunit loss at these temperatures is consistent with the findings of an earlier BIRD study of the protonated S_4^{n+} ions.[58] At the lower charge states, n = 12 and 13, the loss of neutral B represents the only dissociation channel observed, while the loss of protonated B represents the major dissociation channel at n = 16. At n = 14 and 15, B was ejected from the complex in both its neutral and protonated forms. The dissociation pathways observed for all of the charge states investigated are summarized in Scheme 1. Shown in Figure S4 are kinetic plots measured for the dissociation of the $(S_4+4B)^{n+}$ ions at the temperatures indicated. Notably, the plots exhibit excellent linearity, which is consistent with the presence of a single dominant reactant structure at each charge state. The linear plots also indicate that the loss of neutral and protonated B, from the $(S_4+4B)^{n+}$ ions at n = 14 and 15, proceed through parallel pathways. Arrhenius plots were constructed from the $k_{n,app}$, $k_{n,N,ave}$, and $k_{n,C,ave}$ values, which were determined as described in the Data Analysis section. Shown in Figure 3 are the Arrhenius plots, based on the temperature dependence of the $k_{n,app}$ values, for the loss of B from the $(S_4+4B)^{n+}$ ions at n = 12−16. The corresponding plot for the loss of B from the (S_4+4B) complex in aqueous solution at pH 7.4, extrapolated from kinetic data determined at temperatures ranging from 4 to 37 °C,[25] is also shown for comparison. Arrhenius plots based on the $k_{n,N,ave}$ and $k_{n,C,ave}$ values are shown in Figure S5. The Arrhenius parameters (E_a, A; $E_{a,N}$, A_N; and $E_{a,C}$, A_C) are listed in Table 2, as are the parameters for the loss of B from the (S_4+4B) complex in

dx.doi.org/10.1021/ja305213z | J. Am. Chem. Soc. 2012, 134, 16586−16596

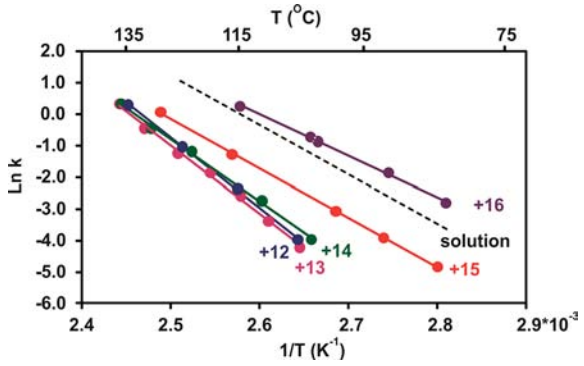

Figure 3. Arrhenius plots for the dissociation of the gaseous WT $(S_4+4B)^{n+}$ ions, where n = 12−16, and the corresponding Arrhenius plot (based on parameters calculated at 110 °C from the activation enthalpy and entropy values reported in ref 25) for the dissociation of the WT (S_4+4B) complex in neutral aqueous solution at pH 7.4.

aqueous solution at pH 7.4, which were calculated from the reported activation enthalpy and entropy.[25]

Inspection of Figure 3 (and Table 2) reveals that the Arrhenius plots for the loss of B from $(S_4+4B)^{n+}$ ions at n = 12 and 13 are nearly indistinguishable, with E_a values of 44 and 43 kcal mol^{-1}, respectively. Taken on their own, these results suggest that B is stabilized by the same or similar intermolecular interactions at these charge states. In contrast, the kinetic stabilities of the $(S_4+4B)^{n+}$ ions, at n = 13−16, decrease with increasing charge state. The trend in kinetic stability mirrors the trend in E_a, which also decreases with increasing charge state. To a first approximation, the decrease in E_a with increasing charge state can be understood in terms of the effect of Coulombic repulsion on the pathway leading to the loss of protonated B. As discussed in detail elsewhere,[58] electrostatic repulsion between the charged products, in this case $(S_4+3B)^{(n-1)+}$ and B^+, will serve to reduce the energy barrier for dissociation, and the magnitude of this effect is expected to increase with the charge state of the complex. Indeed, the $E_{a,C}$ values determined for the loss of protonated B from the $(S_4+4B)^{n+}$ ions at n = 14−16 decrease significantly with increasing charge state (by ∼11 kcal mol^{-1} from +14 to +16). However, the $E_{a,N}$ values for the loss of neutral B from the $(S_4+4B)^{n+}$ ions, at n = 13−15, also decrease by a similar amount. These results indicate that charge-induced structural changes, which alter the intermolecular interactions or reduce their strength or number but do not lead to detectable changes in Ω, occur at these higher charge states.

Kinetic measurements were also performed on $(S_4+4B)^{13+}$ ions composed of five binding site mutants (Trp79Phe, Trp108Phe, Trp120Phe, Ser27Ala, and Tyr43Ala) in order to identify some of the residues that bind to B in the gas phase. In each case, BIRD resulted in the sequential loss of neutral B, similar to what was observed for the WT $(S_4+4B)^{13+}$ ion. Representative kinetic plots, measured at the temperatures indicated, are shown in Figure S6. The Arrhenius plots are shown in Figure S7, and the corresponding parameters are listed in Table 3. Inspection of kinetic parameters reveals that

Table 3. Arrhenius Activation Parameters (E_a, A) Measured for the Loss of B from the Protonated $(S_4+4B)^{13+}$ Ions, Where S_4 Is WT and Trp79Phe, Trp108Phe, Trp120Phe, Ser27Ala, or Tyr43Ala Mutants

S_4	E_a[a] (kcal mol^{-1})	ΔE_a[b] (kcal mol^{-1})	A[a] (s^{-1})
WT	43.2 ± 1.1	–	$10^{23.2\pm0.6}$
Trp79Phe	40.7 ± 0.3	−2.5 ± 1.1	$10^{21.8\pm0.2}$
Trp108Phe	44.8 ± 0.5	1.6 ± 1.2	$10^{24.1\pm0.3}$
Trp120Phe	40.6 ± 0.4	−2.6 ± 1.2	$10^{21.8\pm0.2}$
Ser27Ala	38.5 ± 1.0	−4.7 ± 1.4	$10^{20.7\pm0.6}$
Tyr43Ala	37.8 ± 0.9	−5.4 ± 1.4	$10^{20.4\pm0.5}$

[a]Errors correspond to standard deviations. [b]The values correspond to $\Delta E_a = E_a$(mutant) − E_a(WT).

replacement of Ser27 or Tyr43 with Ala results in a significant decrease, by ∼5.0 kcal mol^{-1}, in E_a. According to the crystal structure, both of these residues participate in H-bonds with B (Figure 1). The magnitude of the reductions in E_a measured upon mutation to Ala is comparable to those observed upon replacement of H-bonding groups (e.g., hydroxyl groups) in the protonated (scFv+αGal[αAbe]αMan)$^{n+}$ ions.[6] Replacement of Trp79 or Trp120, both of which are reported to stabilize B in solution, with Phe also results in a decrease in E_a, although these changes are smaller, ∼2.5 kcal mol^{-1}. Together, these results suggest that Trp79, Trp120, Ser27, and Tyr43 interact with B in the gaseous WT $(S_4+4B)^{13+}$ ion. In contrast, replacement of Trp108 with Phe does not produce a significant change in E_a, suggesting that either Trp108 does not interact with B in the gas phase or, if it does, the interaction is energetically similar to that resulting from the introduction of Phe at this position. Taken together, the results of this mutagenesis study suggest that, at least, some of the stabilizing intermolecular interactions in the (S_4+4B) complex are preserved in the gaseous $(S_4+4B)^{13+}$ ion. This finding is consistent with those reported previously for the protonated

Table 2. Arrhenius Activation Parameters (E_a, A) Measured for the Loss of B from the Protonated $(S_4+4B)^{n+}$ Ions, Where n = 12−16, in the Gas Phase and the Corresponding Parameters Measured for the (S_4+4B) Complex in Aqueous Solution at pH 7.4[a]

n	E_a (kcal mol^{-1})	A (s^{-1})	$E_{a,N}$[c] (kcal mol^{-1})	A_N[c] (s^{-1})	$E_{a,C}$[d] (kcal mol^{-1})	A_C[d] (s^{-1})
12	44.3 ± 0.8	$10^{23.9\pm0.4}$	44.3 ± 0.8	$10^{23.3\pm0.4}$	–	–
13	43.2 ± 1.1	$10^{23.2\pm0.6}$	43.2 ± 1.1	$10^{22.6\pm0.6}$	–	–
14	38.2 ± 0.8	$10^{20.5\pm0.5}$	38.5 ± 1.1	$10^{19.9\pm0.6}$	37.3 ± 1.0	$10^{18.9\pm0.6}$
15	31.2 ± 0.1	$10^{17.0\pm0.2}$	32.2 ± 1.0	$10^{16.0\pm0.6}$	30.7 ± 0.6	$10^{16.0\pm0.3}$
16	26.1 ± 0.4	$10^{14.9\pm0.3}$	–	–	26.1 ± 0.4	$10^{14.2\pm0.3}$
solution	31.2 ± 0.2[b]	$10^{17.6\pm0.1}$[b]				

[a]Errors correspond to standard deviations. [b]E_a and A values calculated at 110 °C from the activation enthalpy and entropy reported in ref 25. [c]The parameters $E_{a,N}$ and A_N correspond to the loss of neutral B from the protonated $(S_4+4B)^{n+}$ ions, where n = 12−16. [d]The parameters $E_{a,C}$ and A_C correspond to the loss of protonated B from the protonated $(S_4+4B)^{n+}$ ions, where n = 12−16.

dx.doi.org/10.1021/ja305213z | J. Am. Chem. Soc. 2012, 134, 16586−16596

(scFv+αGal[αAbe]αMan)$^{n+}$ ions and deprotonated (Lg+FA)$^{7-}$ ions,[6−9] although, for both of these complexes, new (gas-phase) intermolecular interactions were identified for the ions investigated. With the goal of generating a more complete interaction map for the gaseous WT $(S_4+4B)^{13+}$ ion, our laboratory plans to extend these measurements to additional Ala mutants.

Computational Results. In an effort to gain additional insight into the nature of the intermolecular interactions stabilizing the gaseous WT $(S_4+4B)^{12+}$ and $(S_4+4B)^{13+}$ ions, which exhibit similar kinetic stabilities, MD simulations were performed on $(S_4+4B)^{12+}$ ions. The +12 charge state, with the charges partitioned equally between subunits, was selected with the view of simplifying the comparison of the intermolecular interactions in each of the subunits. Uncertainty in the appropriate location of the charges is a major challenge to implementation of MD simulations for gaseous, multiply charged ions of macromolecules and their complexes. In the present study, 15 different charge configurations were considered. In each case, the charges were distributed equally between subunits and placed on Arg, Lys, and His, which have the highest intrinsic gas-phase basicity.[59] A summary of the charge sites considered for the $(S_4+4B)^{12+}$ ions is given in Table S3.

For each charge configuration, the C_α rmsd was calculated with respect to the crystal structure of the (S_4+4B) complex, Table S3. In all cases the values are small, averaging 0.372 ± 0.035 nm. The small C_α rmsd values, which are comparable in size to values reported for other protein complexes in the gas phase,[6,60] suggest relatively minor structural changes accompanying the transfer of the complex from solution to the gas phase, at least at the +12 charge state. At each charge configuration, averaged coordinates were also established, and the corresponding Ω values were calculated, Table S3. Not surprisingly, the Ω values are somewhat sensitive to the charge configuration: the Ω values range from 36.1 to 38.1 nm^2, with an average value of 37.1 ± 0.6 nm^2. Overall, the Ω values agree quite well with the experimental value: the average value is within 8%, and many of the Ω values for individual configurations are within 1−2% of the experimental values. These results suggest that at least some of the structures obtained from the MD simulations may serve as reasonable representations of the gaseous $(S_4+4B)^{12+}$ ion.

The total numbers of H-bonds between streptavidin and B in the $(S_4+4B)^{12+}$ ion at each charge configuration, averaged across all frames and the four subunits, are summarized in Table S3. It can be seen that there is no significant difference in the total number of H-bonds between the different configurations. Across all charge configurations, the average number of H-bonds is 7.2 ± 0.8, which is similar in number to the eight primary H-bonds identified from the crystal structure of the (S_4+4B) complex. However, analysis of the trajectories also reveals that the H-bond donor−acceptor pairs fluctuate over time, differ between subunits, and are sensitive to the charge state configuration. For example, analysis of configuration 12_1 (Table S3) reveals five H-bond pairs that have a fractional occupancy f > 50% in one of the subunits [Tyr43-OH···B-O, Ser45-O···B-N2H, Thr90-OH···B-S, Asp128-O···B-N1H, (adjacent subunit) Lys121-NH_3^+···B-O12] and two [Thr90-OH···B-S, (adjacent subunit) Lys121-NH_3^+···B-O12], two [Asn23-NH_2···B-O, Tyr43-OH···B-O, Thr90-OH···B-S, (adjacent subunit) Lys121-NH_3^+···B-O12], and four H-bond pairs [Ser27-OH···B-O, Tyr43-OH···B-O, Asn49-bb···B-O11, Thr90-OH···B-S] in the other three subunits. The variation in the nature and number of the H-bonds present for the different subunits may reflect structural (crystallographic) differences between subunits, as well as structural differences arising in the heating and equilibrium process. The observation of many other H-bond pairs, with f < 50%, also suggests that the H-bonds are readily broken and replaced with other, energetically similar interactions.

Analysis of all the H-bonds identified among the different charge configurations for the $(S_4+4B)^{12+}$ ion reveals the presence of many different donor−acceptor pairs. However, only eight of these [Asn23-NH_2···B-O, Ser27-OH···B-O, Tyr43-OH···B-O, Ser45-O···B-N2H, Asn49-bb···B-O11, Thr90-OH···B-S, Asp128-O···B-N1H, (adjacent subunit) Lys121-NH_3^+···B-O12] are ever present with f > 50% for a given charge configuration (Figure 1b). On the basis of this analysis, it is proposed that these represent the most probable H-bonds in the gaseous $(S_4+4B)^{12+}$ ion. Interestingly, seven of these H-bonds are also found in the crystal structure of the (S_4+4B) complex (Figure 1a), the only discrepancy being the interaction between Lys121-NH_3^+ from the adjacent subunit and B-O12, which was identified from the simulations. However, when Lys121 is in its neutral form, this interaction (which replaces the H-bond between Ser88-OH and B-O12) is absent.

The trajectories obtained for all of the charge configurations were also analyzed to establish the presence of van der Waals contacts between B and the four tryptophan residues implicated in binding in solution (Trp79, Trp92, Trp108, and Trp120 from adjacent subunit). Notably, all four of these van der Waals interactions exhibit a high f (>80% when averaged over all subunit and all charge configurations), suggesting that they are preserved in the gas phase (Figure 1b).

The results of the MD simulations performed on the $(S_4+4B)^{12+}$ ion suggest that the structure of the ligand binding site does not undergo significant changes when the complex is transferred to the gas phase by ESI. Furthermore, the results suggest that the specific intermolecular interactions, both H-bonds and van der Waals contacts, may survive in the gas phase, although there is also the possibility that new interactions could form. Future efforts will focus on calculating the potential of mean force (PMF)[61] for the escape of B from the binding site in the gas-phase $(S_4+4B)^{n+}$ ions. From the PMF, the dissociation rate constants for the loss of B from the $(S_4+4B)^{n+}$ ions can be computed using transition-state theory.[62] This will allow for a direct comparison of the dissociation kinetics and energetics determined experimentally and predicted theoretically.

Kinetic Stability: Solution versus Gas Phase. The most significant finding of the present study is the observation that the kinetics for the loss of neutral B from the protonated gaseous $(S_4+4B)^{n+}$ ions, at n = 12−14, are dramatically slower at 25 °C than the loss of B from the (S_4+4B) complex in aqueous solution at pH 7.4.[25] For example, the k_{off} at 25 °C for $(S_4+4B)^{13+}$ is 3.1 × 10^{-9} s^{-1} (value extrapolated from the measured Arrhenius plots), compared to 5.4 × 10^{-6} s^{-1} in solution.[27] This is, perhaps, a surprising result, given that the (S_4+4B) complex is among the most kinetically stable protein−ligand complexes known,[27,35,36] and reveals that the streptavidin−biotin interaction has the inherent capacity for even greater stability than previously recognized. As noted above, the enhanced kinetic stability of this interaction in the gas phase, compared to aqueous solution, is the result of a much larger

dissociation E_a. For example, the E_a for the pathway leading to the loss of neutral B, which is not significantly affected by Coulombic repulsion, is as much as 13 kcal mol^{-1} larger than that measured in solution.[25]

As described above, the experimental and theoretical results obtained for the $(S_4+4B)^{n+}$ ions at the lower charge states suggest that many, if not most, of the intermolecular interactions present in solution are preserved in the gas phase. Therefore, it is reasonable to expect that solvent effects are responsible, at least in part, for the difference in E_a values measured for the gaseous $(S_4+4B)^{n+}$ ions and solvated (S_4+4B) complex.[8] If the loss of B from the (S_4+4B) complex, in its hydrated and dehydrated forms, proceeds through similar dissociation pathways in solution and the gas phase, then the difference between E_a in solution ($E_{a,aq}$) and in the gas phase ($E_{a,g}$) will reflect the difference in the hydration enthalpy of the TS ($\Delta H_{hydr,TS}$) and the reactant ($\Delta H_{hydr,R}$):[8]

$$E_{a,aq} - E_{a,g} \approx \Delta H_{hydr,R} - \Delta H_{hydr,TS} \quad (10)$$

Although there is no way to accurately determine the magnitude of the solvent effect, i.e., the ($\Delta H_{hydr,R} - \Delta H_{hydr,TS}$) term, the effect can be estimated in the case where dissociation proceeds through a late TS, wherein the ligand is fully removed from the binding cavity, or nearly so, and assuming no other structural changes accompany ligand loss. In this situation, the magnitude of the solvent effect will reflect the enthalpies of hydration of B and the amino acid residues originally involved in binding.[8]

To our knowledge, the enthalpy of hydration (ΔH_{hyd}) of deprotonated B has not been measured experimentally. However, this value can be estimated from the enthalpy of solution of B in water (ΔH_{sol}) and the enthalpy of vaporization of B to give an ideal gas (ΔH_{vap}), eq 11:[63]

$$\Delta H_{hyd} = \Delta H_{sol} - \Delta H_{vap} \quad (11)$$

The ΔH_{sol} for neutral B has been determined to be 9.7 ± 0.4 kcal mol^{-1}, and the enthalpy of ionization of B is reported to be only 0.3 kcal mol^{-1}.[64] While there is no experimental ΔH_{vap} value for B, it is estimated, using the Joback and Reid Group Contribution Method,[65] to be 20.3 kcal mol^{-1}. On the basis of these values, ΔH_{hyd} of B is estimated to be approximately −10 kcal mol^{-1}. Despite the uncertainty associated with this value, this analysis suggests that the bulk of the difference in E_a values for the loss of B in solution and the gas phase (as a neutral) can be accounted for by the hydration of B in the TS. The remaining energy difference potentially reflects the hydration of the exposed residues within the binding cavity in the TS. It is also possible that structural differences or differences in the mechanisms by which B escapes from the binding site in solution and in the gas phase are reflected in the differences in E_a values measured for the gaseous $(S_4+4B)^{n+}$ ions and the solvated (S_4+4B) complex. The results of the planned mutagenesis study, *vide supra*, will allow for a more definitive conclusion regarding the structural similarities of the hydrated and dehydrated forms of the (S_4+4B) complex. Similarly, a comparison of the PMFs calculated for the escape of B from the gaseous $(S_4+4B)^{n+}$ ions and from the (S_4+4B) complex in aqueous solution will help to establish similarities in the ligand escape pathways in the presence and absence of solvent. These planned computational studies will also provide an important opportunity to test the reliability of available theoretical models for describing protein−ligand interactions, both in the presence and in the absence of solvent.

CONCLUSIONS

In summary, the results of the first detailed study of the structure and kinetic stability of gaseous protonated ions of the (S_4+4B) complex are reported. Collision cross sections measured for the gaseous WT S_4^{n+} and WT $(S_4+4B)^{n+}$ ions, at n = 12−16, are found to agree within 10% of values estimated for the crystal structures for S_4 and (S_4+4B). These results suggest that S_4 and (S_4+4B) complexes do not undergo significant structural changes upon transfer from solution to the gas phase by ESI. A comparison of dissociation E_a for the B loss from the $(S_4+4B)^{13+}$ ions composed of WT and five binding site mutants suggests that at least some of the solution-specific intermolecular interactions are preserved in the gas phase. The results of MD simulations performed on WT $(S_4+4B)^{12+}$ ions with different charge configurations also suggest that the solution-specific intermolecular H-bonds and van der Waals contacts are preserved in the gas phase. The most significant finding of this study is the observation that the gaseous WT $(S_4+4B)^{n+}$ ions at n = 12−14, owing to a much larger E_a (by as much as 13 kcal mol^{-1}) for the loss of B, are dramatically more stable kinetically at 25 °C than the (S_4+4B) complex in aqueous neutral solution. It is shown that the differences in E_a values measured for the gaseous $(S_4+4B)^{n+}$ ions and solvated (S_4+4B) complex can be largely accounted for by the rehydration of B in the dissociative TS.

ASSOCIATED CONTENT

Supporting Information

ESI and BIRD mass spectra, arrival time distributions, kinetic data, Arrhenius plots, and results of MD simulations. This material is available free of charge via the Internet at http://pubs.acs.org.

AUTHOR INFORMATION

Corresponding Author

john.klassen@ualberta.ca

Notes

The authors declare no competing financial interest.

ACKNOWLEDGMENTS

The authors are grateful for financial support provided by the Natural Sciences and Engineering Research Council of Canada and the Alberta Glycomics Centre. The authors acknowledge technical assistance provided by Professors K. Ng (University of Calgary) and P. N. Roy (University of Waterloo), and Professor P. Stayton (University of Washington) for generously providing the plasmid for streptavidin. The MD simulations were made possible by the facilities of the Shared Hierarchical Academic Research Computing Network (SHARCNET:www.sharcnet.ca) and Compute/Calcul Canada.

REFERENCES

(1) Schmidtke, P.; Luque, F. J.; Murray, J. B.; Barril, X. *J. Am. Chem. Soc.* **2011**, *133*, 18903−18910.
(2) Copeland, R. A.; Pompliano, D. L.; Meek, T. D. *Nat. Rev. Drug Discov.* **2006**, *5*, 730−739.
(3) Swinney, D. C. *Curr. Opin. Drug Discov. Dev.* **2009**, *12*, 31−39.
(4) Kitova, E. N.; Bundle, D. R.; Klassen, J. S. *Angew. Chem., Int. Ed.* **2004**, *43*, 4183−4186.

(5) Shoemaker, G. K.; Kitova, E. N.; Palcic, M. M.; Klassen, J. S. *J. Am. Chem. Soc.* **2007**, *129*, 8674−8675.
(6) Kitova, E. N.; Seo, M.; Roy, P.-N.; Klassen, J. S. *J. Am. Chem. Soc.* **2008**, *130*, 1214−1226.
(7) Liu, L.; Bagal, D.; Kitova, E. N.; Schnier, P. D.; Klassen, J. S. *J. Am. Chem. Soc.* **2009**, *131*, 15980−15981.
(8) Liu, L.; Michelsen, K.; Kitova, E. N.; Schnier, P. D.; Klassen, J. S. *J. Am. Chem. Soc.* **2010**, *132*, 17658−17660.
(9) Liu, L.; Michelsen, K.; Kitova, E. N.; Schnier, P. D.; Klassen, J. S. *J. Am. Chem. Soc.* **2012**, *134*, 3054−3060.
(10) Wyttenbach, T.; Bowers, M. T. *Annu. Rev. Phys. Chem.* **2007**, *58*, 511−533.
(11) Xie, Y.; Zhang, J.; Yin, S.; Loo, J. A. *J. Am. Chem. Soc.* **2006**, *128*, 14432−14433.
(12) Hall, Z.; Politis, A.; Bush, M. F.; Smith, L. J.; Robinson, C. V. *J. Am. Chem. Soc.* **2012**, *134*, 3429−3438.
(13) Rose, R. J.; Labrijn, A. F.; van den Bremer, E. T. J.; Loverix, S.; Lasters, I.; van Berkel, P. H. C.; van de Winkel, J. G. J.; Schuurman, J.; Parren, P. W. H. I.; Heck, A. J. R. *Structure* **2011**, *19*, 1274−1282.
(14) Kitova, E. N.; Bundle, D. R.; Klassen, J. S. *J. Am. Chem. Soc.* **2002**, *124*, 5902−5913.
(15) Kitova, E. N.; Bundle, D. R.; Klassen, J. S. *J. Am. Chem. Soc.* **2002**, *124*, 9340−9341.
(16) Zdanov, A.; Li, Y.; Bundle, D. R.; Deng, S. J.; MacKenzie, C. R.; Narang, S. A.; Young, N. M.; Cygler, M. *Proc. Natl. Acad. Sci. U.S.A.* **1994**, *91*, 6423−6427.
(17) Dunbar, R. C.; McMahon, T. B. *Science* **1998**, *279*, 194−197.
(18) Price, W. D.; Schnier, P. D.; Jockusch, R. A.; Strittmatter, E. F.; Williams, E. R. *J. Am. Chem. Soc.* **1996**, *118*, 10640−10644.
(19) Chaiet, L.; Wolf, F. J. *Arch. Biochem. Biophys.* **1964**, *106*, 1−5.
(20) Hendrickson, W. A.; Pähler, A.; Smith, J. L.; Satow, Y.; Merritt, E. A.; Phizackerley, R. P. *Proc. Natl. Acad. Sci. U.S.A.* **1989**, *86*, 2190−2194.
(21) Stenkamp, R. E.; Trong, I. L.; Klumb, L.; Stayton, P. S.; Freitag, S. *Protein Sci.* **1997**, *6*, 1157−1166.
(22) Le Trong, I.; Wang, Z.; Hyre, D. E.; Lybrand, T. P.; Stayton, P. S.; Stenkamp, R. E. *Acta Crystallogr., Sect. D: Biol. Crystallogr* **2011**, *67*, 813−821.
(23) Hyre, D. E.; Le Trong, I.; Merritt, E. A.; Eccleston, J. F.; Green, N. M.; Stenkamp, R. E.; Stayton, P. S. *Protein Sci.* **2006**, *15*, 459−467.
(24) Freitag, S.; Chu, V.; Penzotti, J. E.; Klumb, L. A.; To, R.; Hyre, D.; Le Trong, I.; Lybrand, T. P.; Stenkamp, R. E.; Stayton, P. S. *Proc. Natl. Acad. Sci. U.S.A.* **1999**, *96*, 8384−8389.
(25) Klumb, L. A.; Chu, V.; Stayton, P. S. *Biochemistry* **1998**, *37*, 7657−7663.
(26) Hyre, D. E.; Stayton, P. S.; Trong, I. L.; Freitag, S.; Stenkamp, R. E. *Protein Sci.* **2000**, *9*, 878−885.
(27) Chilkoti, A.; Stayton, P. S. *J. Am. Chem. Soc.* **1995**, *117*, 10622−10628.
(28) Chu, V.; Stayton, P. S.; Freitag, S.; Le Trong, I.; Stenkamp, R. E. *Protein Sci.* **1998**, *7*, 848−859.
(29) Magalhães, M. L. B.; Czekster, C. M.; Guan, R.; Malashkevich, V. N.; Almo, S. C.; Levy, M. *Protein Sci.* **2011**, *20*, 1145−1154.
(30) Cerutti, D. S.; Trong, I. L.; Stenkamp, R. E.; Lybrand, T. P. *J. Phys. Chem. B* **2009**, *113*, 6971−6985.
(31) DeChancie, J.; Houk, K. N. *J. Am. Chem. Soc.* **2007**, *129*, 5419−5429.
(32) Dixit, S. B.; Chipot, C. *J. Phys. Chem. A* **2001**, *105*, 9795−9799.
(33) Li, Q.; Gusarov, S.; Evoy, S.; Kovalenko, A. *J. Phys. Chem. B* **2009**, *113*, 9958−9967.
(34) Stayton, P. S.; Freitag, S.; Klumb, L. A.; Chilkoti, A.; Chu, V.; Penzotti, J. E.; To, R.; Hyre, D.; Le Trong, I.; Lybrand, T. P.; Stenkamp, R. E. *Biomol. Eng.* **1999**, *16*, 39−44.
(35) Green, N. M. *Adv. Protein Chem.* **1975**, *29*, 85−133.
(36) Piran, U.; Riordan, W. J. *J. Immunol. Methods* **1990**, *133*, 141−143.
(37) Hyre, D.; Amon, L. M.; Penzotti, J. E.; Trong, I. L.; Stenkamp, R. E.; Lybrand, T. P.; Stayton, P. S. *Nat. Struct. Biol.* **2002**, *9*, 582−585.
(38) Chilkoti, A.; Tan, P. H.; Stayton, P. S. *Proc. Natl. Acad. Sci. U.S.A.* **1995**, *92*, 1754−1758.
(39) Sun, J.; Kitova, E. N.; Klassen, J. S. *Anal. Chem.* **2006**, *79*, 416−425.
(40) Bagal, D.; Kitova, E. N.; Liu, L.; El-Hawiet, A.; Schnier, P. D.; Klassen, J. S. *Anal. Chem.* **2009**, *81*, 7801−7806.
(41) Case, D. A.; Darden, T. A.; Cheatham, T. E., III; Simmerling, C. L.; Wang, J.; Duke, R. E.; Luo, R.; Walker, R. C.; Zhang, W.; Merz, K. M.; Roberts, B.; Wang, B.; Hayik, S.; Roitberg, A.; Seabra, G.; Kolossváry, I.; Wong, K. F.; Paesani, F.; Vanicek, J.; Liu, J.; Wu, X.; Brozell, S. R.; Steinbrecher, T.; Gohlke, H.; Cai, Q.; Ye, X.; Wang, J.; Hsieh, M.-J.; Cui, G.; Roe, D. R.; Mathews, D. H.; Seetin, M. G.; Sagui, C.; Babin, V.; Luchko, T.; Gusarov, S.; Kovalenko, A.; Kollman, P. A. *AMBER 11*; University of California, San Francisco, 2010.
(42) Ramasubbu, N.; Ragunath, C.; Mishra, P. J.; Thomas, L. M.; Gyémánt, G.; Kandra, L. *Eur. J. Biochem.* **2004**, *271*, 2517−2529.
(43) Holm, L.; Rosenström, P. *Nucleic Acids Res.* **2010**, *38*, W545−W549.
(44) Vanquelef, E.; Simon, S.; Marquant, G.; Garcia, E.; Klimerak, G.; Delepine, J. C.; Cieplak, P.; Dupradeau, F.-Y. *Nucleic Acids Res.* **2011**, *39*, W511−W517.
(45) Dupradeau, F.-Y.; Pigache, A.; Zaffran, T.; Savineau, C.; Lelong, R.; Grivel, N.; Lelong, D.; Rosanski, W.; Cieplak, P. *Phys. Chem. Chem. Phys.* **2010**, *12*, 7821−7839.
(46) Frisch, M. J.; Trucks, G. W.; Schlegel, H. B.; Scuseria, G. E.; Robb, M. A.; Cheeseman, J. R.; Scalmani, G.; Barone, V.; Mennucci, B.; Petersson, G. A.; Nakatsuji, H.; Caricato, M.; Li, X.; Hratchian, H. P.; Izmaylov, A. F.; Bloino, J.; Zheng, G.; Sonnenberg, J. L.; Hada, M.; Ehara, M.; Toyota, K.; Fukuda, R.; Hasegawa, J.; Ishida, M.; Nakajima, T.; Honda, Y.; Kitao, O.; Nakai, H.; Vreven, T.; Montgomery, J. A., Jr.; Peralta, J. E.; Ogliaro, F.; Bearpark, M.; Heyd, J. J.; Brothers, E.; Kudin, K. N.; Staroverov, V. N.; Kobayashi, R.; Normand, J.; Raghavachari, K.; Rendell, A.; Burant, J. C.; Iyengar, S. S.; Tomasi, J.; Cossi, M.; Rega, N.; Millam, J. M.; Klene, M.; Knox, J. E.; Cross, J. B.; Bakken, V.; Adamo, C.; Jaramillo, J.; Gomperts, R.; Stratmann, R. E.; Yazyev, O.; Austin, A. J.; Cammi, R.; Pomelli, C.; Ochterski, J. W.; Martin, R. L.; Morokuma, K.; Zakrzewski, V. G.; Voth, G. A.; Salvador, P.; Dannenberg, J. J.; Dapprich, S.; Daniels, A. D.; Farkas, Ö.; Foresman, J. B.; Ortiz, J. V.; Cioslowski, J.; Fox, D. J. *Gaussian 09*, Revision A.1; Gaussian, Inc.: Wallingford, CT, 2009.
(47) Wang, J.; Wang, W.; Kollman, P. A.; Case, D. A. *J. Mol. Graphics Modell.* **2006**, *25*, 247−260.
(48) Duan, Y.; Wu, C.; Chowdhury, S.; Lee, M. C.; Xiong, G.; Zhang, W.; Yang, R.; Cieplak, P.; Luo, R.; Lee, T.; Caldwell, J.; Wang, J.; Kollman, P. *J. Comput. Chem.* **2003**, *24*, 1999−2012.
(49) Wang, J.; Wolf, R. M.; Caldwell, J. W.; Kollman, P. A.; Case, D. A. *J. Comput. Chem.* **2004**, *25*, 1157−1174.
(50) Bush, M. F.; Hall, Z.; Giles, K.; Hoyes, J.; Robinson, C. V.; Ruotolo, B. T. *Anal. Chem.* **2010**, *82*, 9557−9565.
(51) Ruotolo, B. T.; Benesch, J. L. P.; Sandercock, A. M.; Hyung, S.-J.; Robinson, C. V. *Nat. Protoc.* **2008**, *3*, 1139−1152.
(52) Uetrecht, C.; Rose, R. J.; van Duijn, E.; Lorenzen, K.; Heck, A. J. R. *Chem. Soc. Rev.* **2010**, *39*, 1633−1655.
(53) Wildgoose, J.; Giles, K.; Pringle, S.; Koeniger, S.; Valentine, S.; Bateman, R.; Clemmer, D. *Abstracts of papers*, Proceedings of the 54th ASMS Conference on Mass Spectrometry and Allied Topics, Seattle, WA; American Society for Mass Spectrometry: Washington, DC, 2006; Abstract 064.
(54) Mesleh, M. F.; Hunter, J. M.; Shvartsburg, A. A.; Schatz, G. C.; Jarrold, M. F. *J. Phys. Chem.* **1996**, *100*, 16082−16086.
(55) University of Illinois at Urbana-Champaign. VMD software home page, http://www.ks.uiuc.edu/Research/vmd/ (accessed Dec 21, 2011).
(56) Phillips, J. C.; Braun, R.; Wang, W.; Gumbart, J.; Tajkhorshid, E.; Villa, E.; Chipot, C.; Skeel, R. D.; Kalé, L.; Schulten, K. *J. Comput. Chem.* **2005**, *26*, 1781−1802.
(57) University of Illinois at Urbana-Champaign. NAMD software home page, http://www.ks.uiuc.edu/Research/namd/ (accessed Dec 21, 2011).

(58) Sinelnikov, I.; Kitova, E. N.; Klassen, J. S. *J. Am. Soc. Mass Spectrom.* **2007**, *18*, 617−631.
(59) Hunter, E. P. L.; Lias, S. G. *J. Phys. Chem. Ref. Data* **1998**, *27*, 413−656.
(60) Patriksson, A.; Marklund, E.; van der Spoel, D. *Biochemistry* **2007**, *46*, 933−945.
(61) Kirkwood, J. G. *J. Chem. Phys.* **1935**, *3*, 300−313.
(62) Schenter, G. K.; Kathmann, S. M.; Garrett, B. C. *J. Chem. Phys.* **1999**, *110*, 7951−7959.
(63) Nilsson, S. O.; Wadsö, I. *J. Chem. Thermodyn.* **1986**, *18*, 673−681.
(64) Suurkuusk, J.; Wadsö, I. *Eur. J. Biochem.* **1972**, *28*, 438−441.
(65) Joback, K. G.; Reid, R. C. *Chem. Eng. Commun.* **1987**, *57*, 233−243.